

Electronic Supplementary Information (ESI)

Structure-dependent iron-based metal-organic frameworks for selectively CO₂-to-CH₄ photocatalytic reduction

Xiao-Yao Dao,[‡] Jin-Han Guo,[‡] Xiao-Yu Zhang, Shi-Qing Wang, Xiao-Mei Cheng and Wei-Yin Sun*

Coordination Chemistry Institute, State Key Laboratory of Coordination Chemistry, School of Chemistry and Chemical Engineering, Nanjing National Laboratory of Microstructures, Collaborative Innovation Center of Advanced Microstructures, Nanjing University, Nanjing 210023, China

E-mail: sunwy@nju.edu.cn

Experimental procedures

Chemicals

Trimesic acid (BTC), terephthalic acid (BDC), trimethyl 1,3,5-benzenetricarboxylate (BtcMe₃) and iron chloride hexahydrate (FeCl₃·6H₂O), triethanolamine (TEOA), and n-tetrabutylammonium hexafluorophosphate [(n-Bu)₄N(PF₆)] were purchased from Aladdin Industrial Corporation, Cr(NO₃)₃·9H₂O, Al(NO₃)₃·9H₂O and iron net were obtained from Sinopharm Chemical Reagent Co., Ltd. Acids and solvents such as hydrofluoric acid (HF ≥40%), nitric acid (HNO₃ 65-68%), N,N-dimethylformamide (DMF), acetonitrile (CH₃CN) and ethanol (EtOH) were obtained from Sinopharm Chemical Reagent Co., Ltd. Nafion PFSA polymer dispersion D520 (5%) was purchased from Dupont China Holding Co., LTD. Deionized (DI) water with a resistivity of above 18.2 MΩ·cm was obtained using a JL-RO100

Millipore-Q Plus water purifier and used throughout the experiments. All chemicals are of analytical grade and used directly without further purification.

Synthesis of MIL-100(Fe)

MIL-100(Fe) was synthesized by a previously reported hydrothermal method with tiny modifications.¹ 2*2 cm (about 90 mg) of the iron net and 63 mg of BTC were mixed in 10 mL of deionized water, followed by addition of 40 μ L of HNO₃ and 24 μ L of HF. The suspension was ultrasonicated at room temperature for 30 min. Subsequently, the mixture was retained at 150 °C for 48 h in a Teflon-lined stainless steel autoclave (30 mL). After cooling naturally, the obtained precipitate was recovered by filtration, washed sequentially by stirring in 80 °C hot deionized water for 6 h and reflux in hot ethanol for 3 h to remove the residual unreacted reactants and colored impurities. Finally, the obtained solids were dried by freeze-drying equipment for further characterization and investigation.

Syntheses of Fe-MOFs: MIL-53(Fe), MIL-88B(Fe) and MIL-101(Fe).

MIL-53(Fe), MIL-88B(Fe) and MIL-101(Fe) were synthesized according to the literature with some modifications.² MIL-101(Fe) was prepared by reaction of H₂BDC (16.6 mg) with FeCl₃·6H₂O (54.1 mg) in DMF (10 mL) at 110 °C for 24 h. MIL-88B(Fe) was prepared similarly to MIL-101(Fe) except for the addition of methanol (2 mL) to DMF (8 mL). As for MIL-53(Fe), H₂BDC and FeCl₃·6H₂O (83 and 135.2 mg) were dissolved in deionized (DI) water (10 mL) and stirred for 30 min, and then the mixture was transferred to a Teflon-lined autoclave for the hydrothermal treatment at 150 °C for 24 h. After being cooled to room temperature, the resultant precipitates were separated by centrifugation and washed thoroughly with DMF and ethanol. Then, the sediment was soaked in EtOH with reflux for 24 h in order to perform exchange of the guest solvent molecules with EtOH and collected by centrifugation. Finally, the obtained solids were dried by freeze-drying equipment for further characterization and investigation.

Synthesis of MIL-100(Al)

The MIL-100(Al) was synthesized by a previously reported hydrothermal method with tiny modifications.³ BtcMe₃ (195 mg) and Al(NO₃)₃·9H₂O (435 mg) were added into H₂O (5 mL), followed by the addition of 100 μL of HNO₃. The suspension was ultrasonicated at room temperature for 30 min. Subsequently, the mixture was retained at 160 °C for 12 h in a Teflon-lined stainless steel autoclave (18 mL). After cooling naturally, the obtained yellowish powdered was recovered by filtration, washed sequentially by stirring in 80 °C hot deionized water for 6 h and reflux in hot ethanol for 3 h to remove the residual unreacted reactants and the colored impurities. Finally, the obtained solids were dried by freeze-drying equipment for further characterization and investigation.

Synthesis of MIL-100(Cr)

The MIL-100(Cr) was synthesized by a previously reported hydrothermal method with a tiny modifications.⁴ BTC (156 mg) and Cr(NO₃)₃·9H₂O (401 mg) were added into H₂O (5 mL), followed by the addition of 100 μL of HF. The suspension was ultrasonicated at room temperature for 30 min. Subsequently, the mixture was retained at 180 °C for 96 h in a Teflon-lined stainless steel autoclave (30 mL). After cooling naturally, the obtained yellowish powdered was recovered by filtration, washed sequentially by stirring in 80 °C hot deionized water for 6 h and reflux in hot ethanol for 3 h to remove the residual unreacted reactants and the colored impurities. Finally, the obtained solids were dried by freeze-drying equipment for further characterization and investigation.

Characterization

The phase and crystalline structures were characterized by powder X-ray diffraction (PXRD) (Bruker D8 Advance X-ray diffractometer) with Cu K α radiation (1.5478 Å). The morphology and microstructural observations were carried out on field emission scanning electron microscope (FE-SEM) (Hitachi S-4800) at an acceleration voltage of 5 kV. X-ray

photoelectron spectroscopy (XPS) was measured on UIVAC-PHI 5000 VersaProbe using a monochromatized Al K α X-ray source, in which all of the binding energies were calibrated with reference to the C 1s peak (284.8 eV). UV-Vis diffuse reflectance spectra were recorded on a Shimadzu UV-3600 spectrophotometer in the wavelength range of 200 - 800 nm (BaSO₄ purchased from Sigma-Aldrich was used as reference). The photoelectrochemical measurements were carried out on an electrochemical workstation (CHI730E, Shanghai Chenhua Limited, China), and the electrochemical impedance spectroscopy was carried out on Zahner electrochemical workstation (IM6ex, Zahner Scientific Instruments, German). ¹H-NMR spectra were measured on Bruker-DRX 500 MHz instruments at room temperature. The time-resolved photoluminescence (PL) decay spectra were recorded on HORIBA FL-3 spectrometer. Gas (N₂, CO₂) sorption properties and the specific surface area (BET) were measured on a Micromeritics ASAP 2020. Before measurements, the samples were degassed at 160 °C for 8 h under vacuum of 10⁻⁵ bar. The N₂ adsorption isotherms were monitored at 77 K, while CO₂ adsorption isotherms were obtained at 273 and 298 K. The temperature-programmed desorption of CO (CO-TPD) was carried out on a Micromeritics Chemisorb 2920.

Isosteric Analysis of Sorption Heat Using Langmuir model.⁵

$$q = n \frac{bp}{1 + bp} \quad (1)$$

$$q = n_1 \frac{b_1 p}{1 + b_1 p} + n_2 \frac{b_2 p}{1 + b_2 p} \quad (2)$$

In the two formulas, the (1) represents single-site Langmuir model, and the (2) represents dual-site Langmuir model. Here q is adsorption capacity, p is pressure, n , n_1 and n_2 are the numbers of adsorption sites, and b , b_1 and b_2 are Langmuir constants.

Solar-to-Methane (CH₄) Conversion Efficiency.⁶

The CH₄ conversion yield was calculated as follows:

$$\eta(\%) = \frac{R(\text{CH}_4) \times \Delta G}{P \times S} \quad (3)$$

$R(\text{CH}_4)$, ΔG , P , and S denote the rate of methane evolution (mol s^{-1}) in the photocatalytic system, the change in the Gibbs free energy that accompanies CO_2 photoreduction to CH_4 , the energy intensity of the light irradiation (0.4 W cm^{-2}), and the irradiation area (2.8 cm^2), respectively. Thus, the conversion efficiency of the MIL-100(Fe) was calculated to be 0.023%.

Quantum Efficiency Measurements.^{6,7}

The apparent quantum efficiency (AQY%) is defined as the ratio of the number of reacted electrons to the number of incident photons.

The general equation is given below:

$$\text{AQY}\% = \frac{\text{Number of Reacted Electrons}}{\text{Number of Incident Photons}} \times 100\% = \frac{8 \times Y(\text{CH}_4) \times N_A + 2 \times Y(\text{CO}_2) \times N_A}{\theta \times T \times S} \times 100\% \quad (4)$$

In the formula, $Y(\text{CH}_4)$ and $Y(\text{CO}_2)$ are the yield of CH_4 and CO_2 for the catalyst, N_A is Avogadro's number, θ is the incident photon, T is the irradiation time, S is the illumination area.

The calculation result is based on the data with MIL-100(Fe) for 5h: $Y(\text{CH}_4)$ is $2.37 \times 10^{-4} \text{ mol}$, $Y(\text{CO})$ is $0.196 \times 10^{-4} \text{ mol}$, N_A is $6.022 \times 10^{23} \text{ mol}^{-1}$, T is 5 hours, and S is 2.8 cm^2 ; the incident photons (θ) is $2.46 \times 10^{18} \text{ s}^{-1} \text{ cm}^{-2}$. For photocatalyst of MIL-100(Fe): $\text{AQY}\% = \{ (8 \times 2.37 \times 10^{-4} + 2 \times 0.196 \times 10^{-4}) \times 6.022 \times 10^{23} \} / (2.46 \times 10^{18} \times 5 \times 3600 \times 2.8) = 0.943\%$.

Turnover frequency (TOF) of the catalysts:

The product conversion yield was calculated as follows:

$$\text{TOF} = \frac{n(\text{Products})}{n(\text{M})} \times t \quad (5)$$

In the formula, $n(\text{Product})$ is the amount of product (mol) detected by GC, $n(\text{M})$ is the amount of metal ions of the catalyst (mol) and t is the reaction time (s).

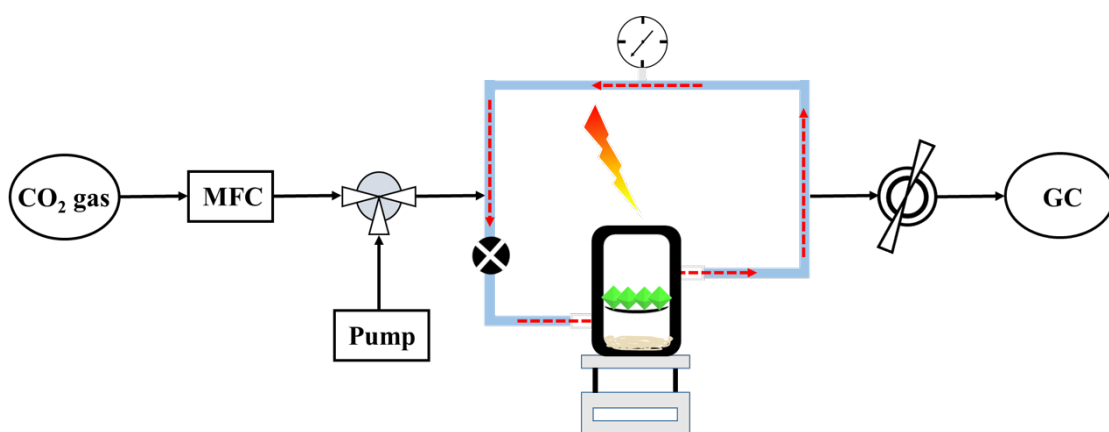


Fig. S1 Photocatalytic CO₂ reduction in a solvent-free system.

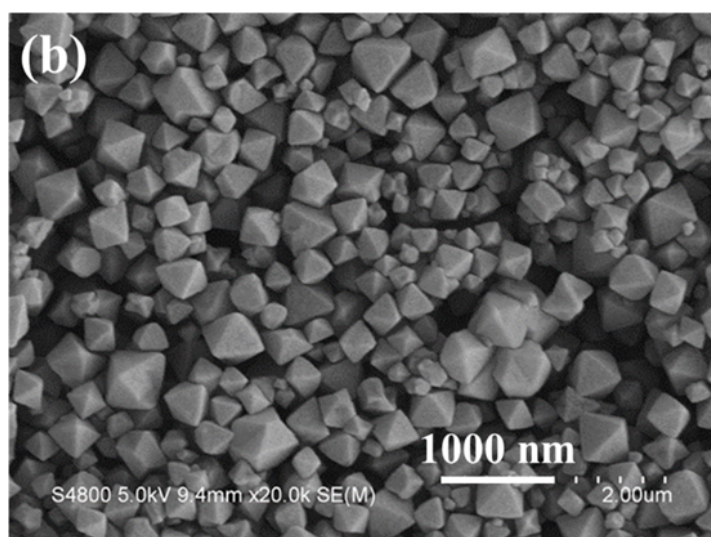
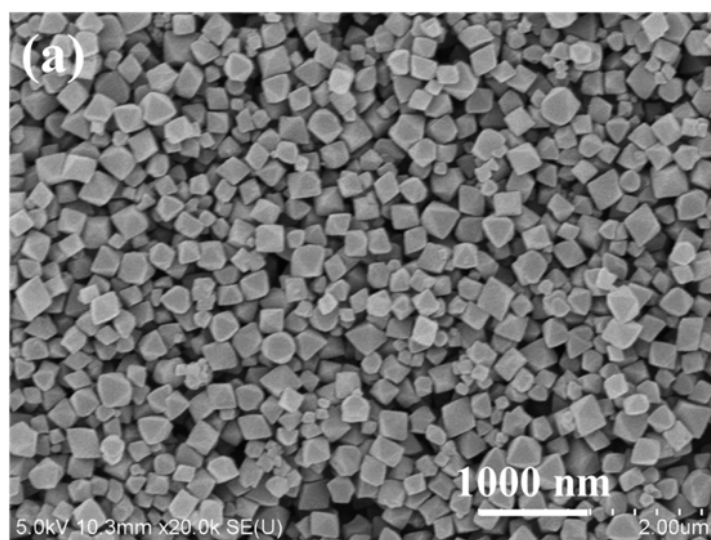


Fig. S2 SEM images of MIL-100(Fe) (a) and MIL-101(Fe) (b).

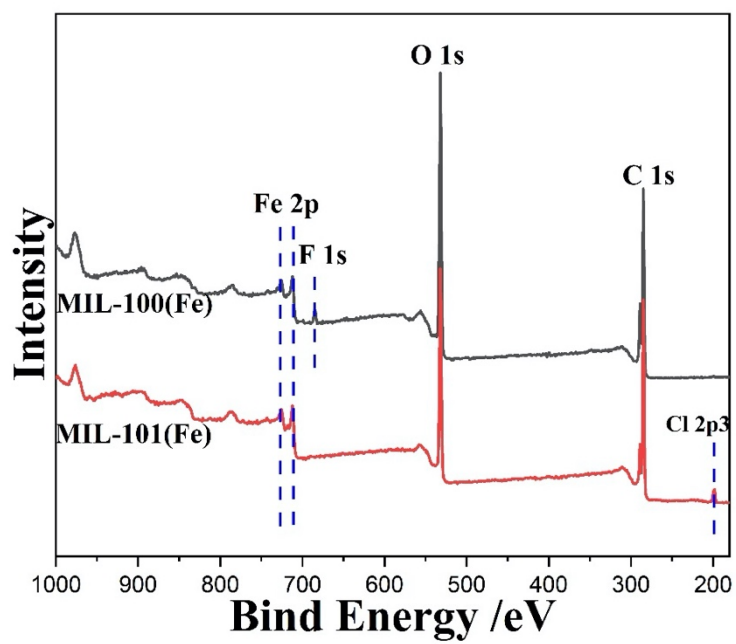


Fig. S3 XPS spectra of MIL-100(Fe) and MIL-101(Fe): survey spectra.

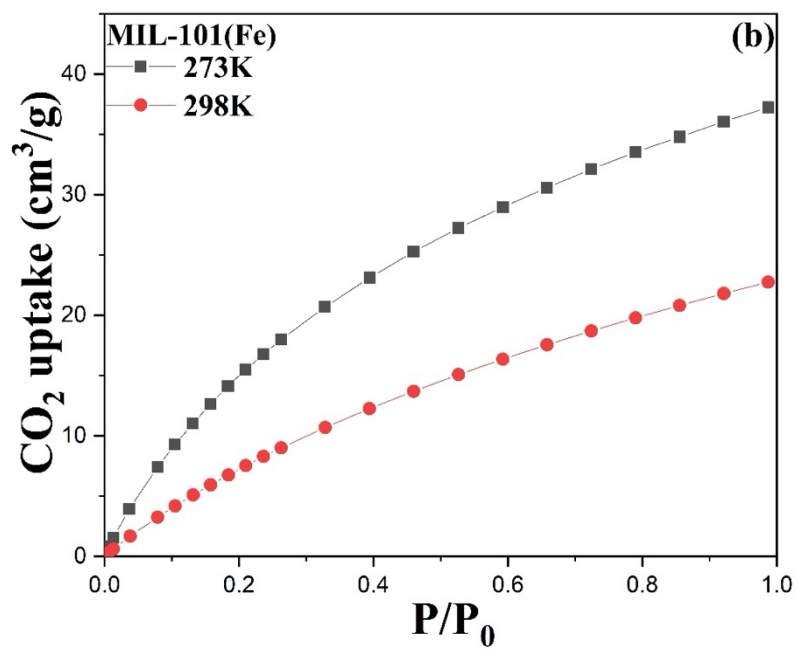
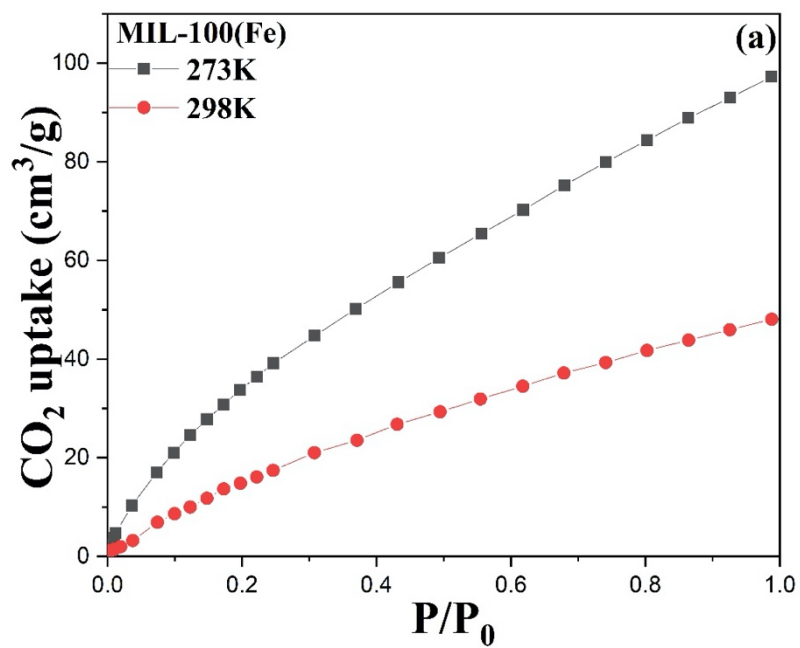


Fig. S4 CO₂ adsorption isotherms at 273 and 298 K of MIL-100(Fe) (a) and MIL-101(Fe) (b).

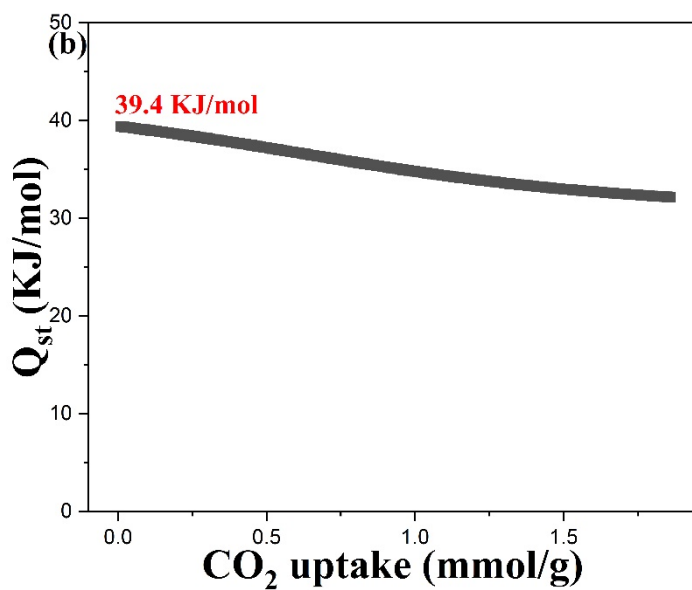
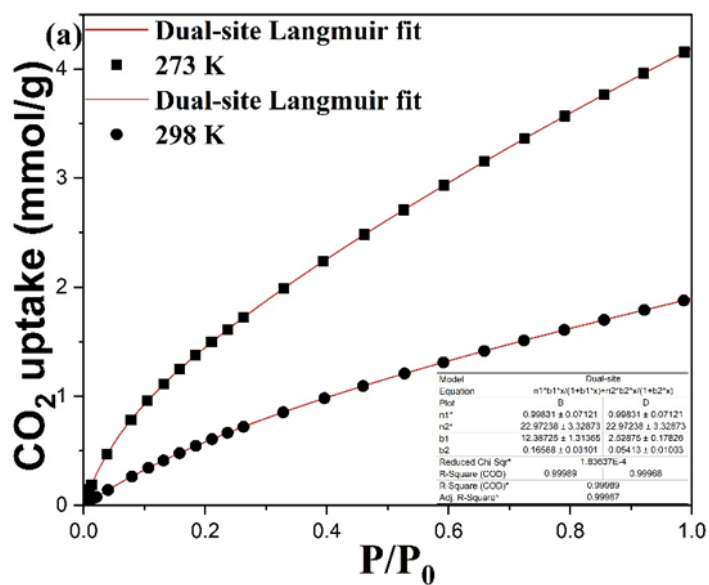


Fig. S5 (a) The calculated dual-sites Langmuir model isotherms parameters fit the experimental CO₂ data of MIL-100(Fe). (b) CO₂ adsorption heat calculated by the Langmuir model of MIL-100(Fe).

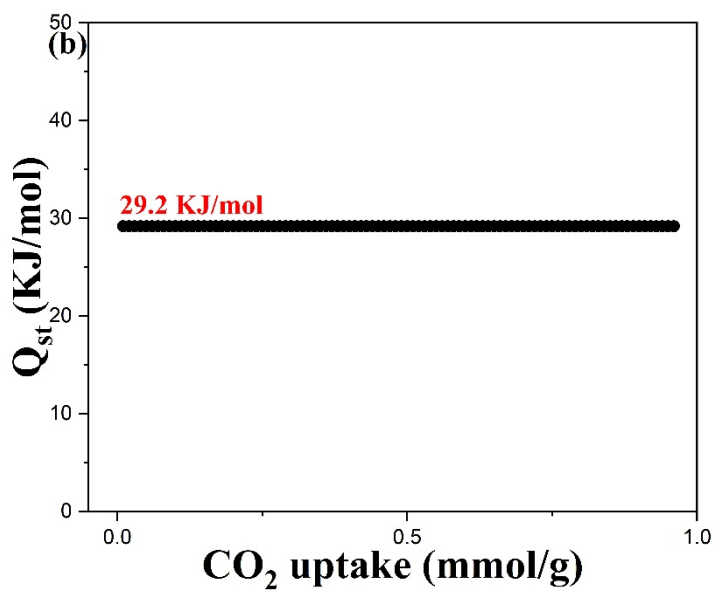
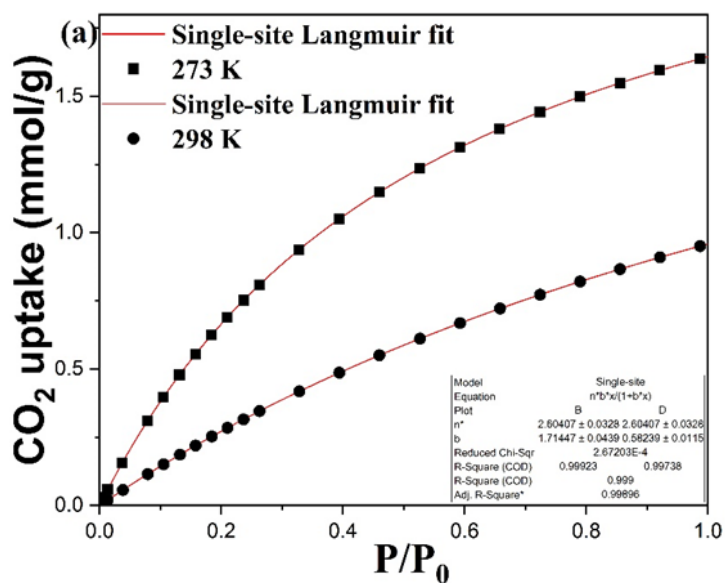


Fig. S6 (a) The calculated single-sites Langmuir model isotherms parameters fit the experimental CO₂ data of MIL-101(Fe). (b) CO₂ adsorption heat calculated by the Langmuir model of MIL-101(Fe).

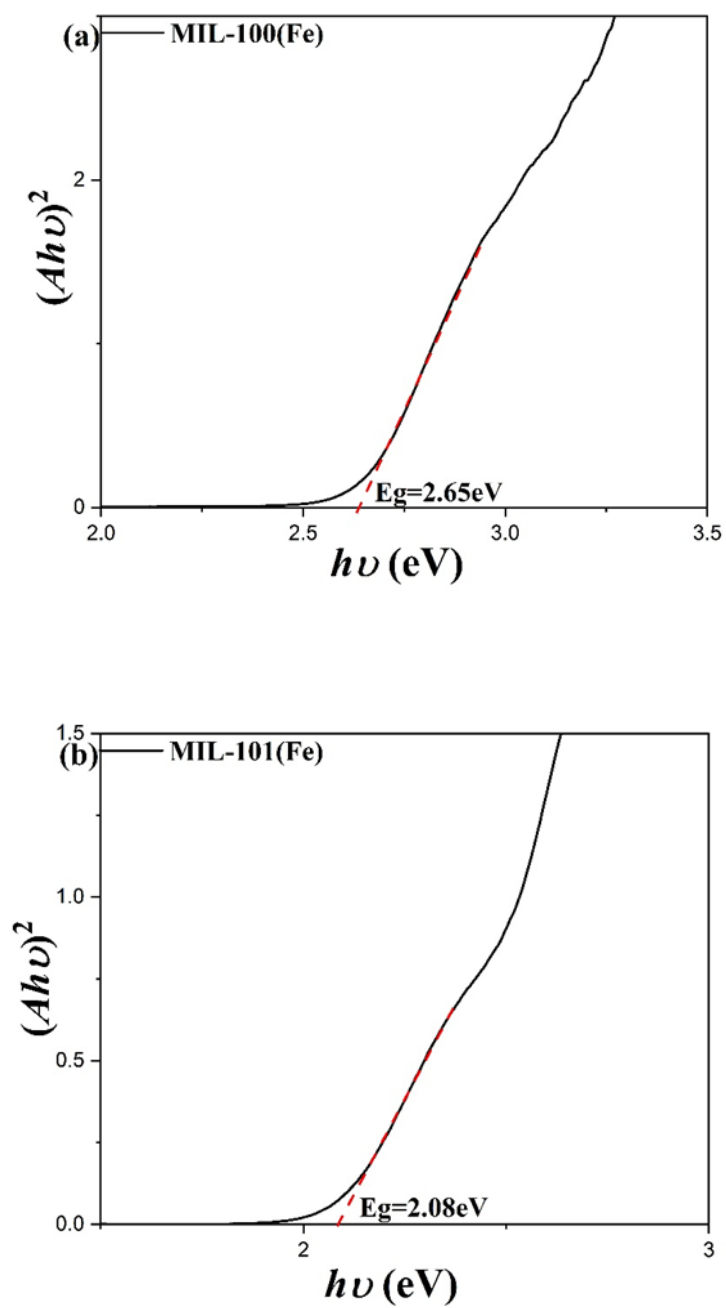


Fig. S7 Plots of $(Ah\nu)^2$ vs photon energy for MIL-100(Fe) (a), and MIL-101(Fe) (b).

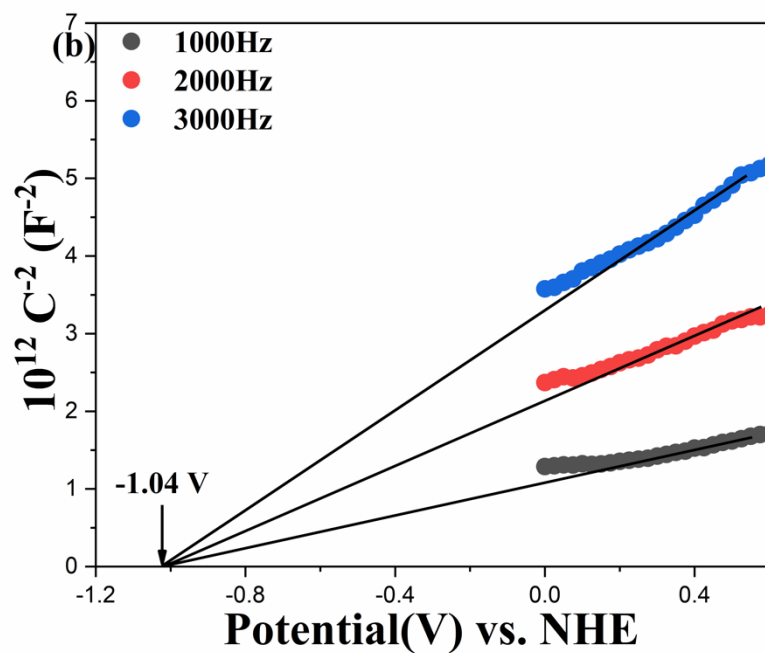
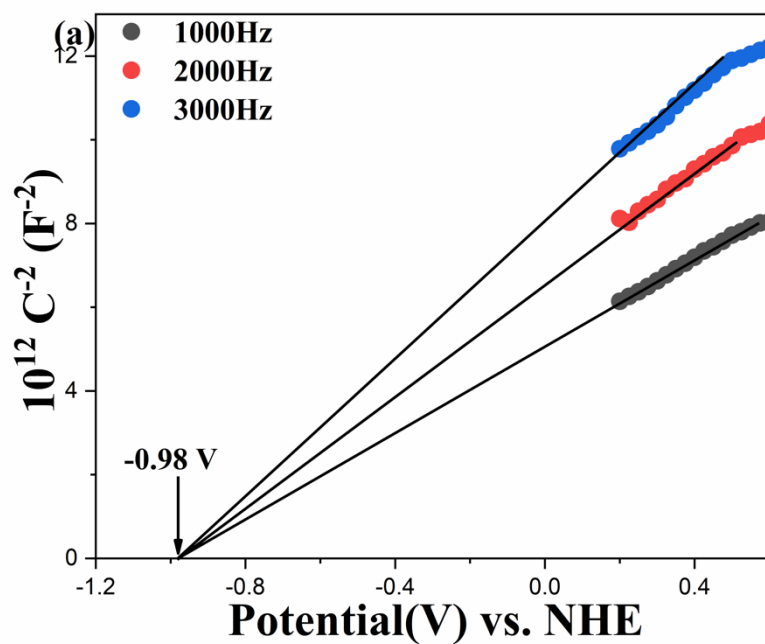


Fig. S8 Mott-Schottky plots of MIL-100(Fe) (a), and MIL-101(Fe) (b).

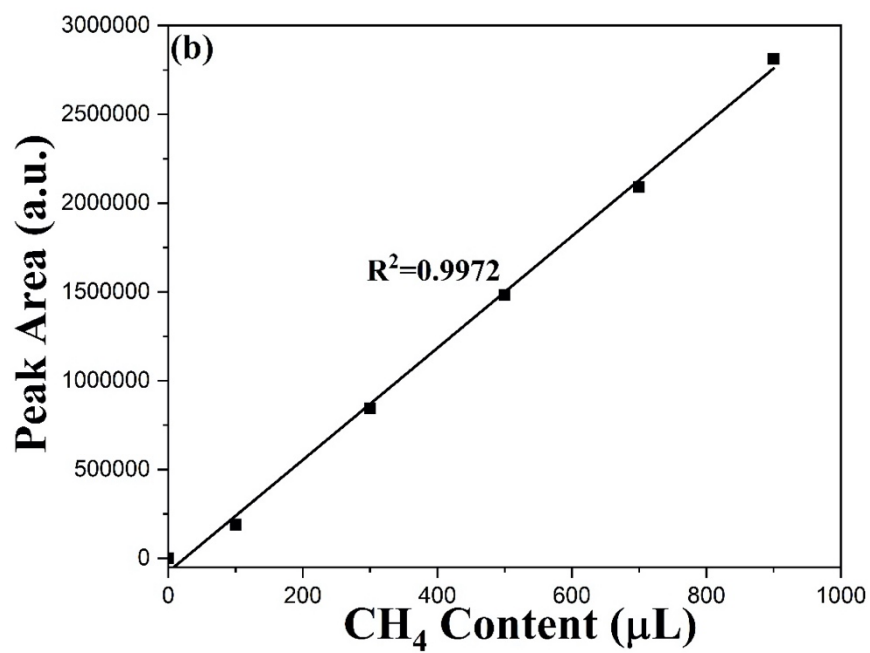
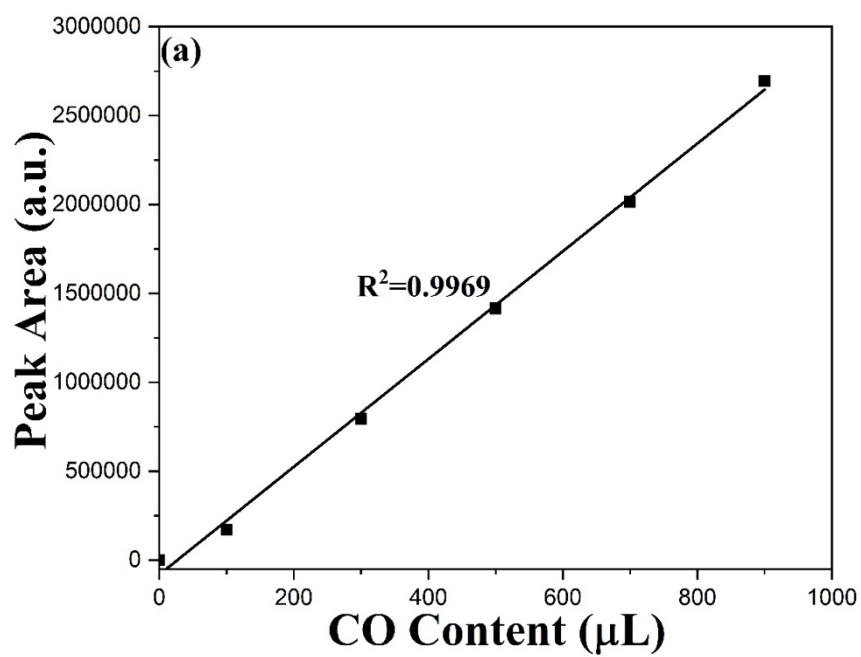


Fig. S9 GC calibration curves for CO (a) and CH_4 (b) under different contents.

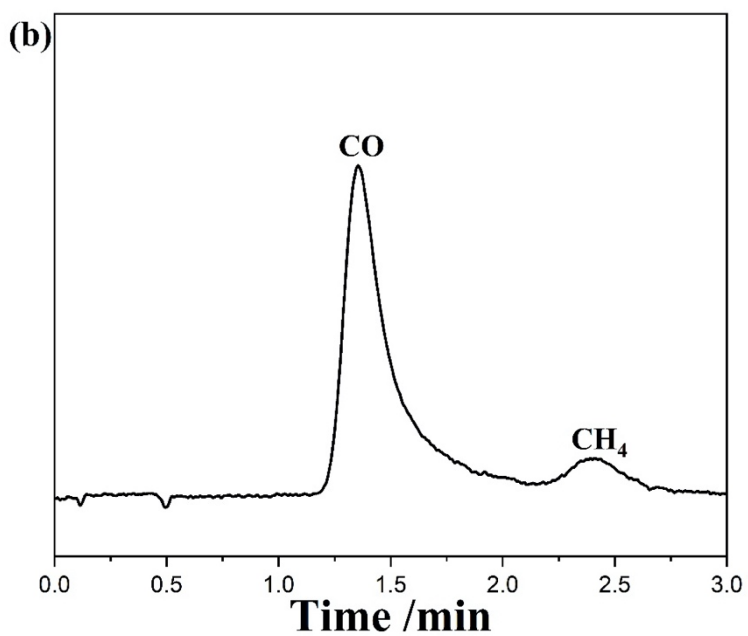
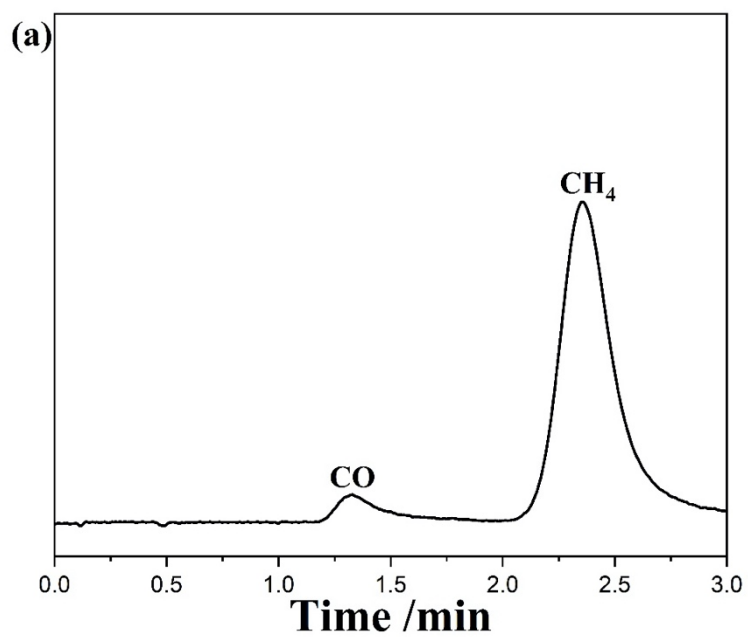


Fig. S10 The gas products including CH₄ and CO were detected by gas chromatogram: MIL-100(Fe) (a), and MIL-101(Fe) (b).

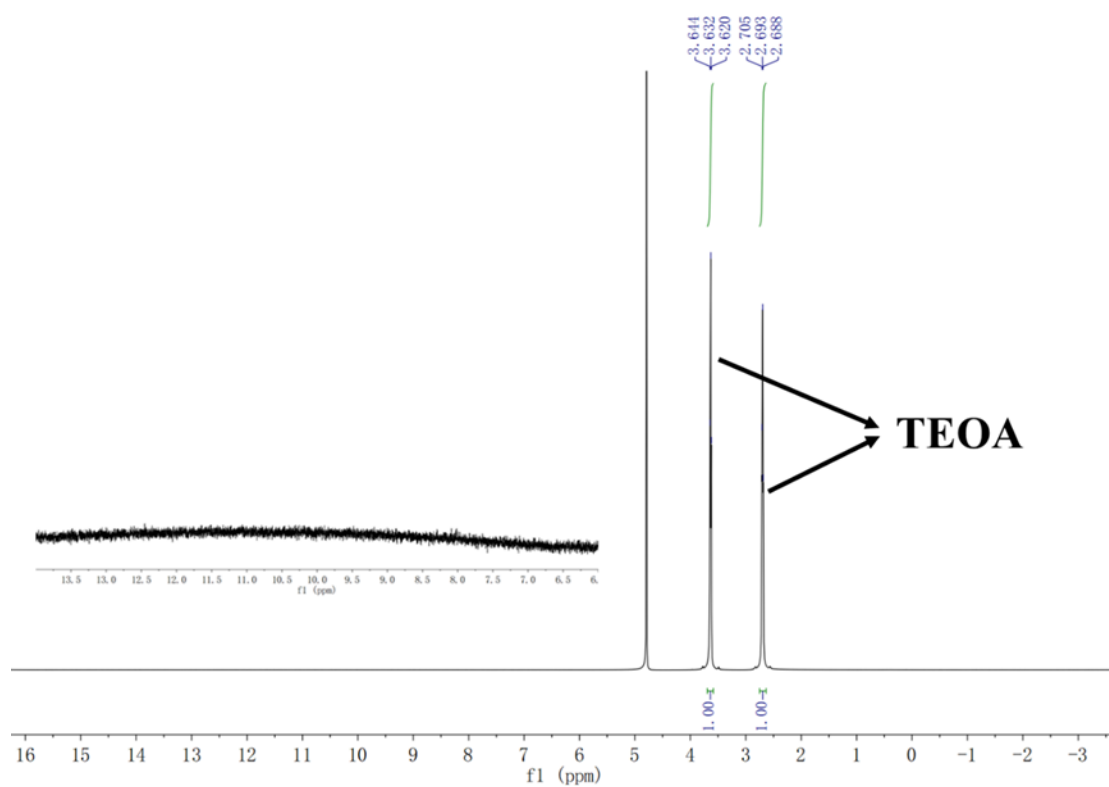


Fig. S11 ^1H NMR spectrum applied to detect the liquid products (such as HCOOH and CH_3OH) from the photocatalytic CO_2 reduction.

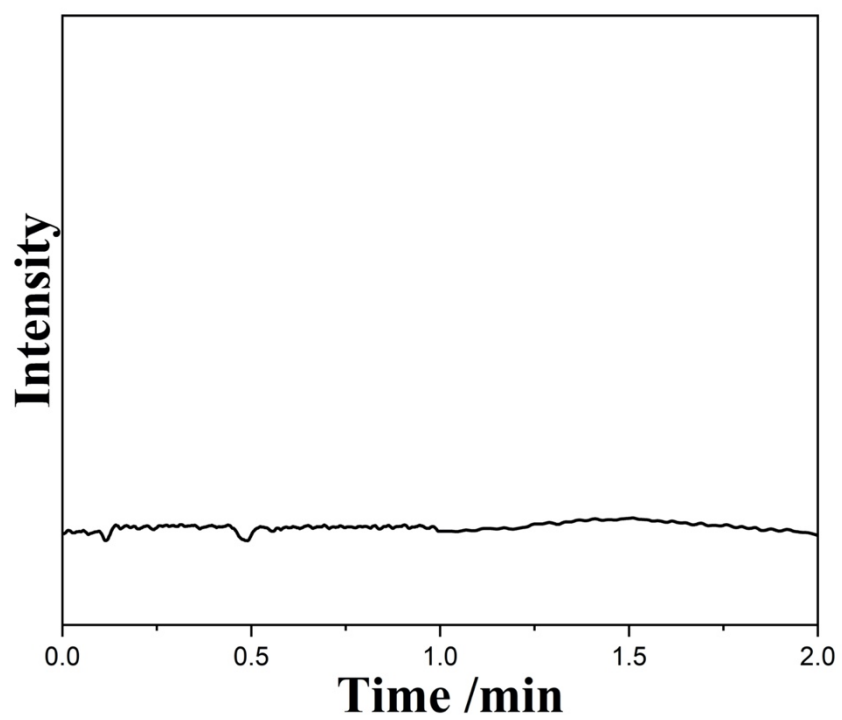


Fig. S12 The gaseous products upon visible-light irradiation analyzed by gas chromatograms: TCD detector for H₂ detection, indicating no H₂ produced.

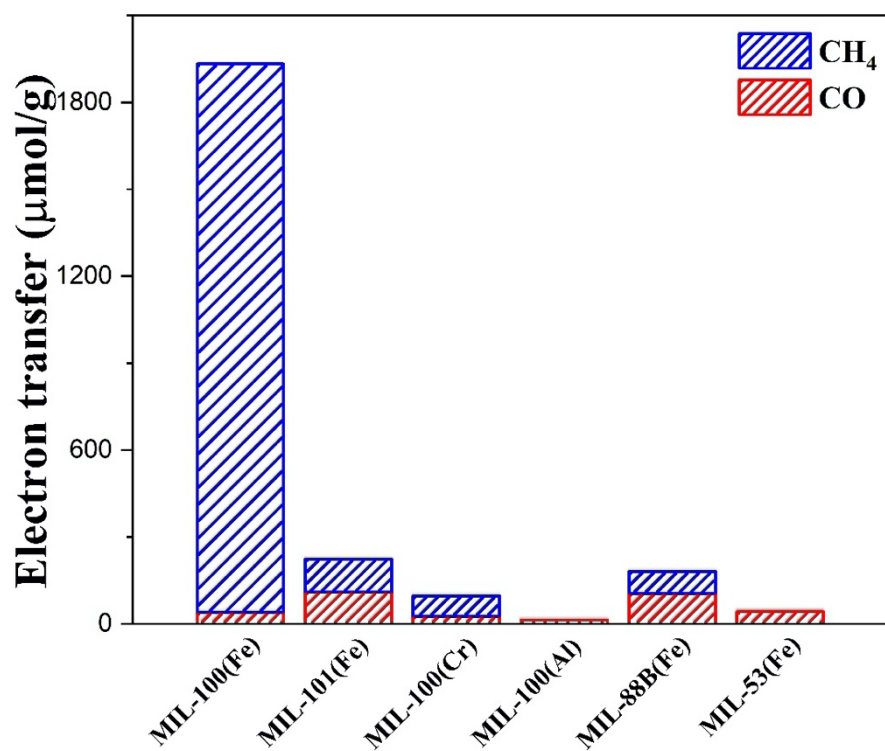


Fig. S13 Photocatalytic CO_2 reduction evaluation over different catalysts: the reacted electrons' yields.

Table S1. Comparison of the photocatalytic activities of the reported heterogeneous photocatalysts.

Photocatalyst	Light	Photosensitizer	Sacrificial agent	Solvent	Products	AQY (total %)	Reference
MIL-100	Visible light	/	TEOA	/	CH ₄ CO	0.943	This work
MIL-101	Visible light	/	TEOA	/	CH ₄ CO	0.109	This work
NH ₂ -MIL-101	Visible light	/	TEOA	/	CO	0.17	2
NH ₂ -MIL-101	Visible light	/	TEOA	MeCN	HCOOH	0.013 (450nm)	8
MAF-X27-OH	420nm	[Ru(bpy) ₃]Cl·6H ₂ O	TEOA	MeCN/H ₂ O (4:1, v/v)	CO	0.93	9
MAF-X27-Cl	420nm	[Ru(bpy) ₃]Cl·6H ₂ O	TEOA	MeCN/H ₂ O (4:1, v/v)	CO	0.21	9
MAF-X27-OH	420nm	[Ru(bpy) ₃]Cl·6H ₂ O	TEOA	MeCN/H ₂ O (4:1, v/v)	CO	2.0	9
MAF-X27-Cl	420nm	[Ru(bpy) ₃]Cl·6H ₂ O	TEOA	MeCN/H ₂ O (4:1, v/v)	CO	0.39	9
NNU-13	Visible light	/	TEOA	Water	CH ₄	0.04 (550nm)	10
NNU-14	Visible light	/	TEOA	Water	CH ₄	0.02 (550nm)	10
Ru(II)-Re(I) dinuclear complex	480nm	/	BIH	DMF-TEOA (5:1 v/v)	CO	0.5	11
LaPO ₄ -1wt%Pt	UV light	/	Water	Water	CH ₄ H ₂	0.15	12
V _s -CuIn ₃ S ₈	Visible light	/	Water vapor	/	CH ₄	0.786	6

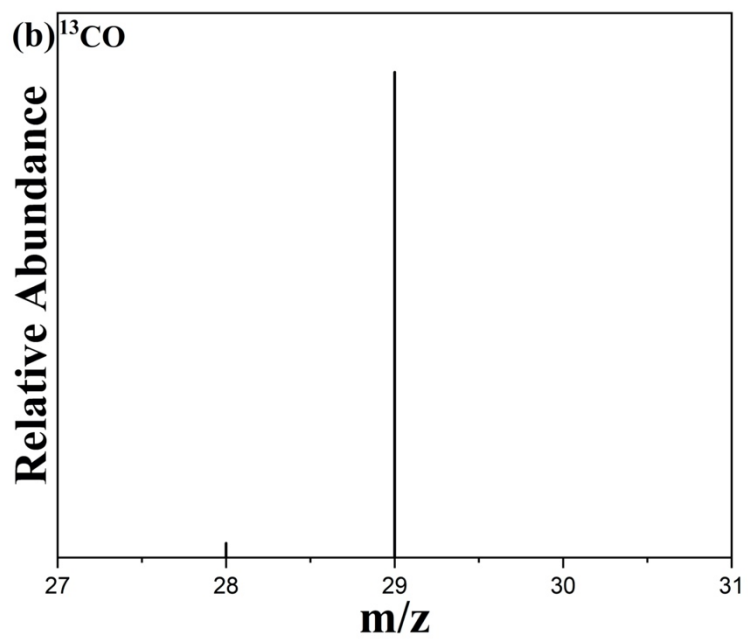
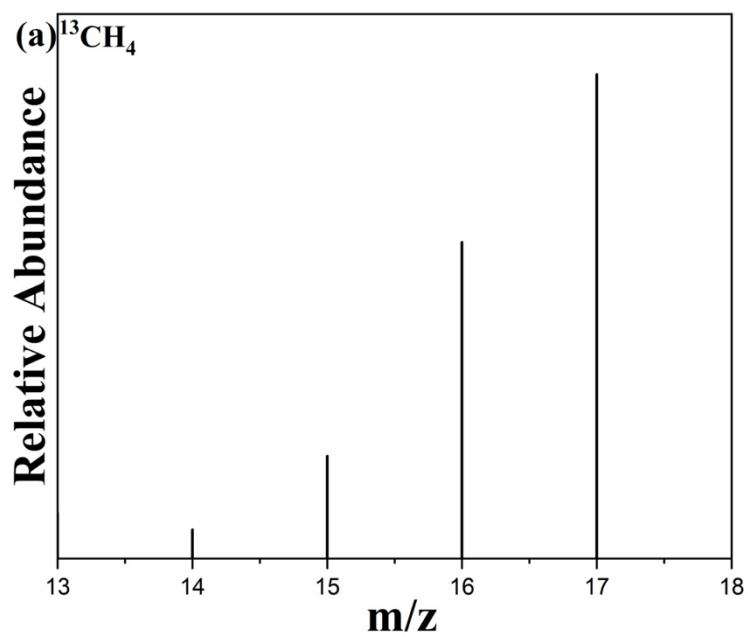


Fig. S14 Mass spectrum of the target products generated from the photoreduction of $^{13}\text{CO}_2$ isotopic experiment: (a) $^{13}\text{CH}_4$ and (b) ^{13}CO .

Table S2. Comparison of MIL-100(Fe), MIL-101(Fe), and NH₂-MIL-101(Fe) photocatalytic CO₂ reduction performances with different CO-yield and CH₄-yield after reaction time 5 h.

	CO($\mu\text{mol}\cdot\text{g}^{-1}$)	CH₄($\mu\text{mol}\cdot\text{g}^{-1}$)
MIL-100(Fe)	19.6	236.7
MIL-101(Fe)	54.4	14.3
MIL-88B(Fe)	32.4	9.5
NH ₂ -MIL-101(Fe)	87.6	/

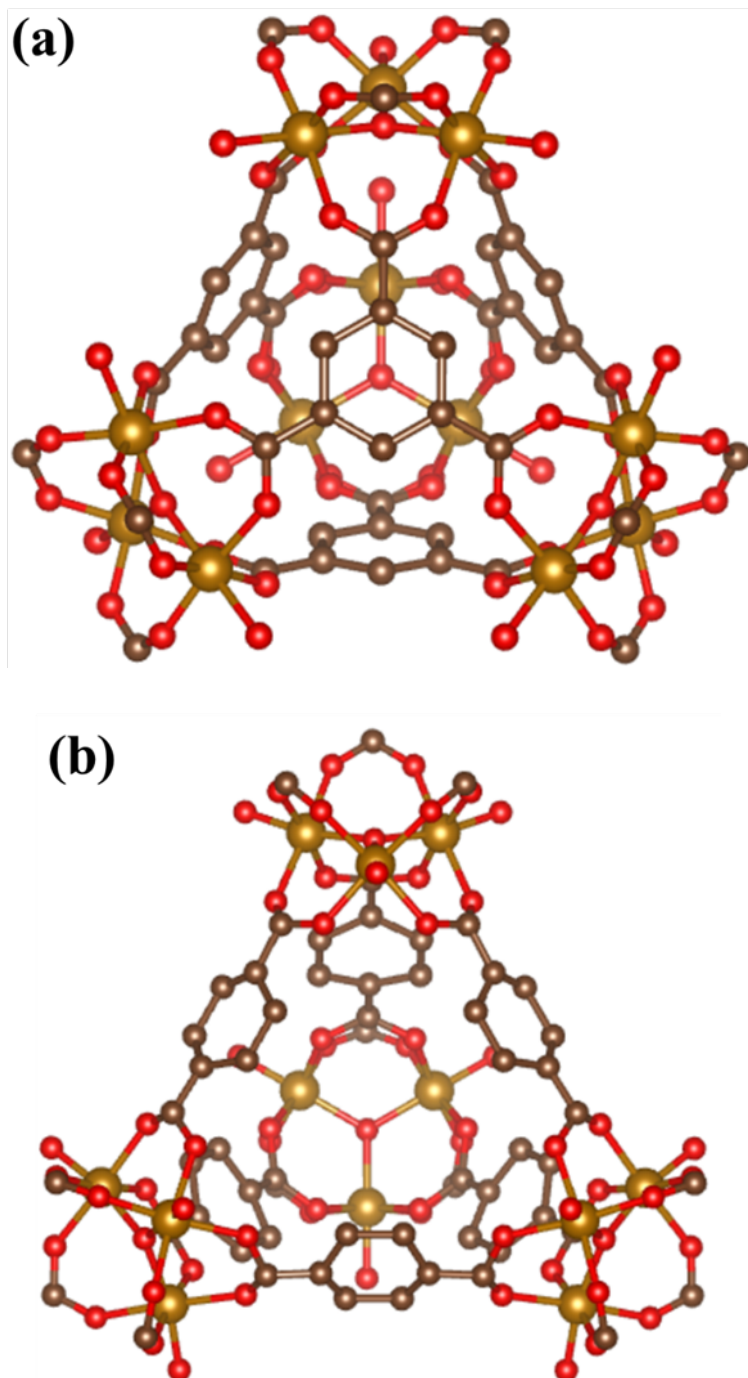


Fig. S15 Structures of MIL-100(Fe) (a), MIL-101(Fe)/NH₂- MIL-101(Fe) (b).

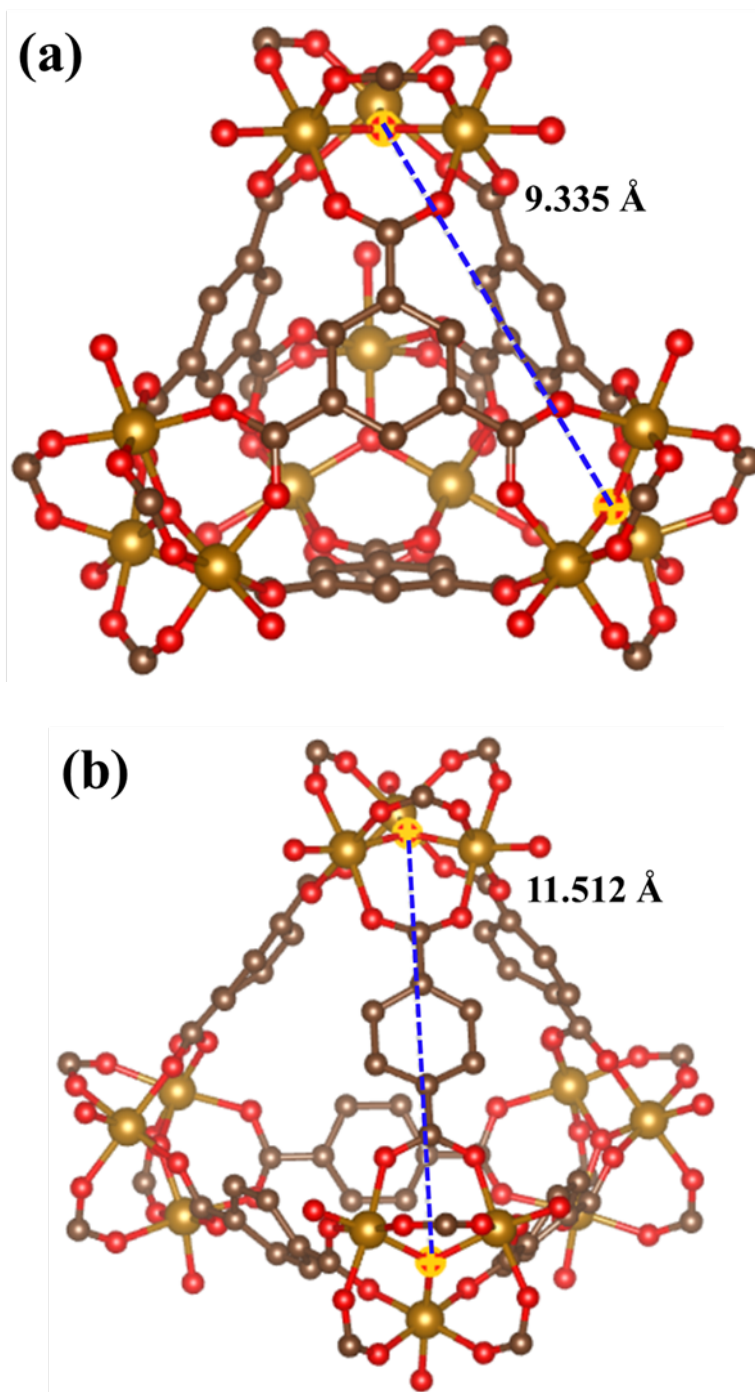


Fig. S16 Distance of adjacent Fe_3O clusters of MIL-100(Fe) (a), MIL-101(Fe)/ NH_2 -MIL-101(Fe) (b).

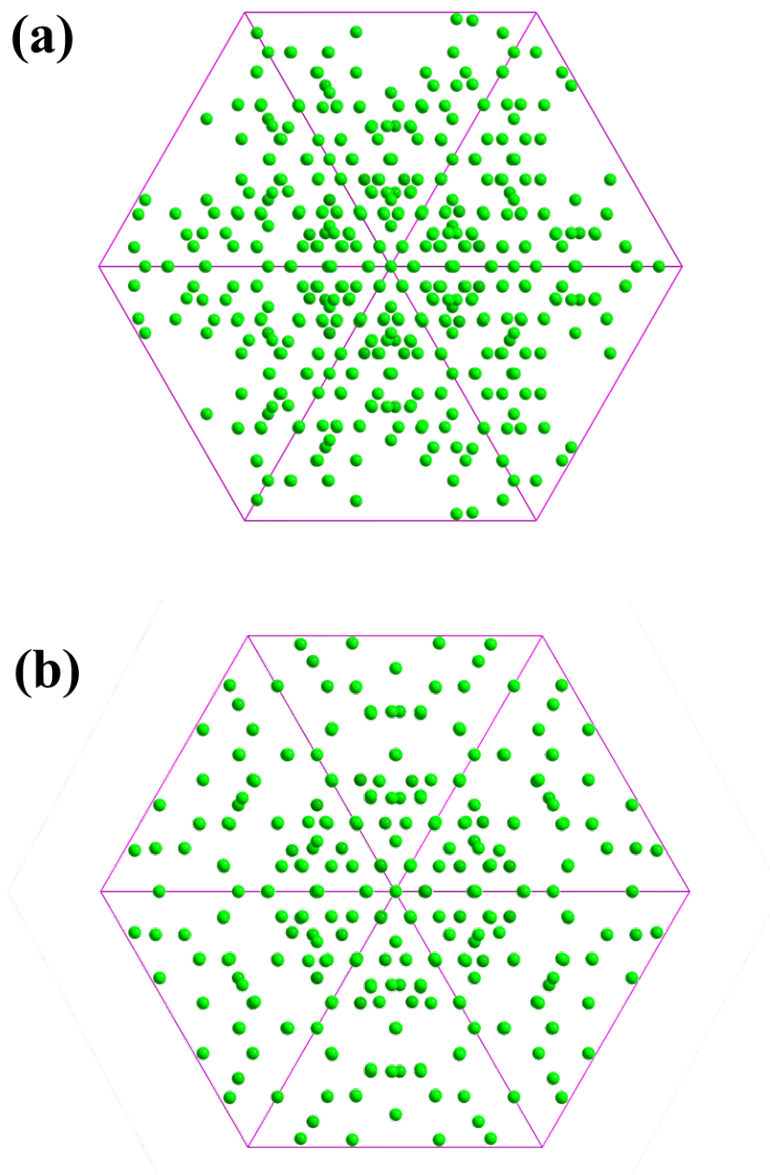


Fig. S17 Density of Fe₃O clusters of MIL-100(Fe) (a), MIL-101(Fe)/NH₂- MIL-101(Fe) (b) with an equivalent photocatalytic area (green ball stands for Fe₃O clusters).

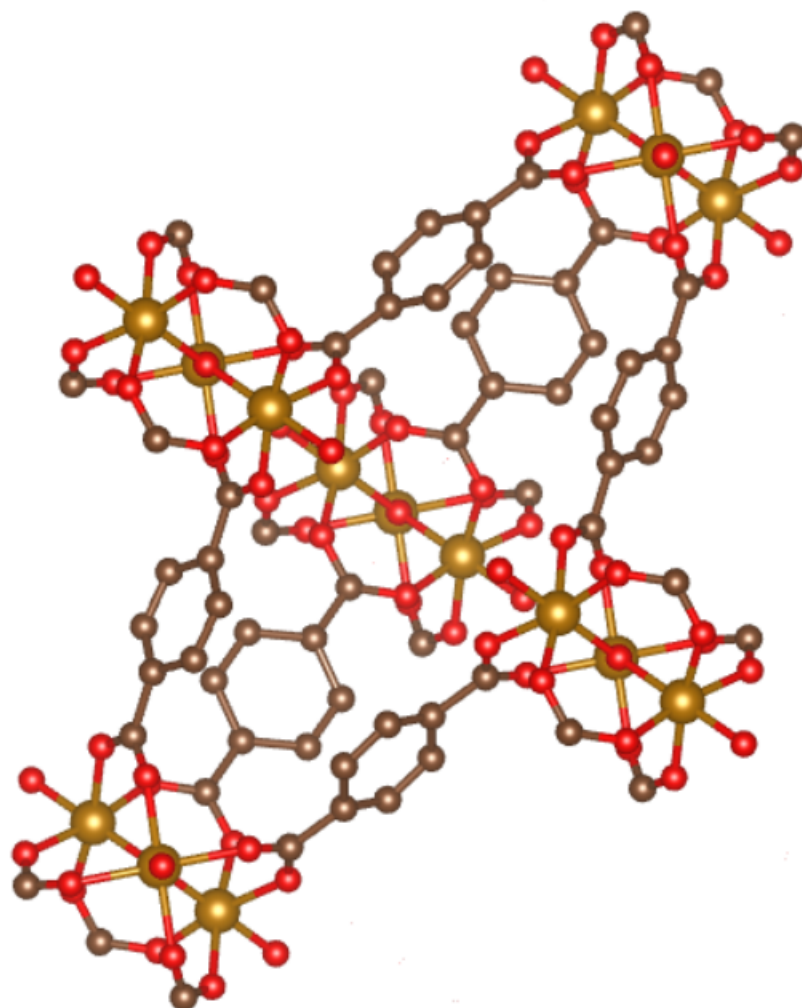


Fig. S18 Structure of MIL-88B(Fe).

Table S3. Photocatalytic reduction CO₂ to CO and CH₄ in various reaction conditions.

Entry	Catalyst	CO ₂	Light	TEOA	CO ($\mu\text{mol}\cdot\text{g}^{-1}$)	CH ₄ ($\mu\text{mol}\cdot\text{g}^{-1}$)
1	/	+	+	+	n.d.	n.d.
2	+	/	+	+	n.d.	n.d.
3	+	+	/	+	n.d.	n.d.
4	+	+	+	/	n.d.	n.d.

“+” stands for presence, “/” stands for inexistence, n.d. = not detectable.

Standard reaction conditions: catalyst (5 mg), CO₂ (80 kPa, 99.999%), TEOA (2 mL), visible light (300 W xenon arc lamp), reaction time 5 h.

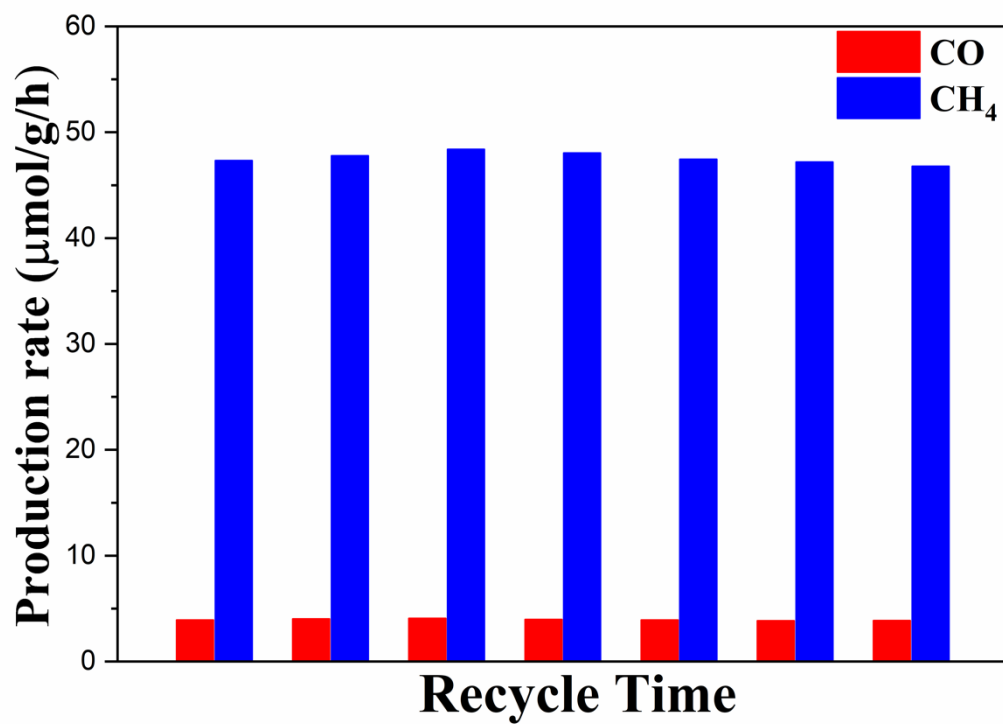


Fig. S19 CO and CH₄ yields of optimal photocatalyst MIL-100(Fe) for successive seven cycles.

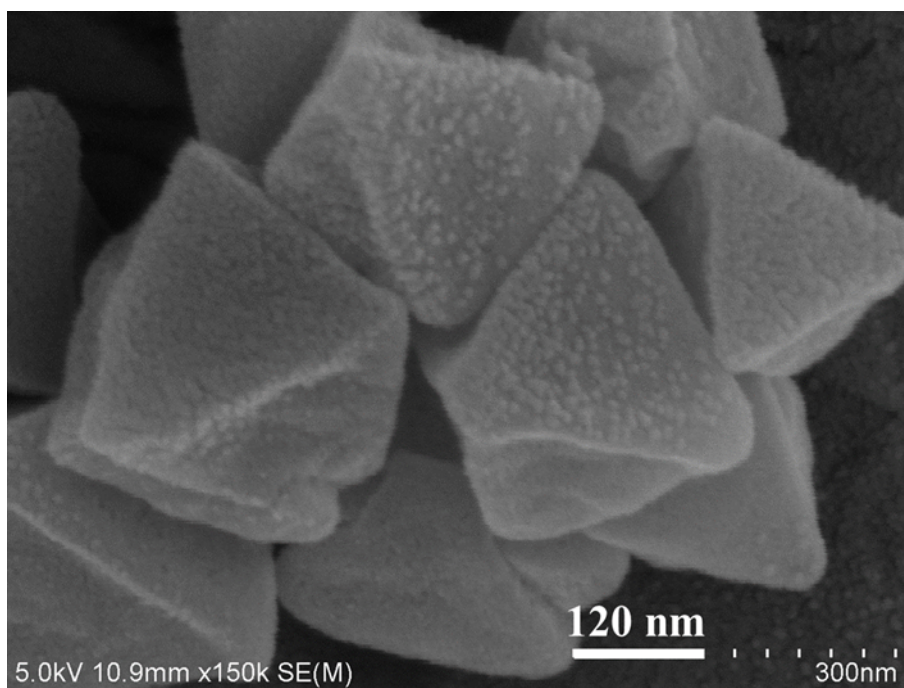


Fig. S20 SEM image of MIL-100(Fe) after successive seven cycle experiments.

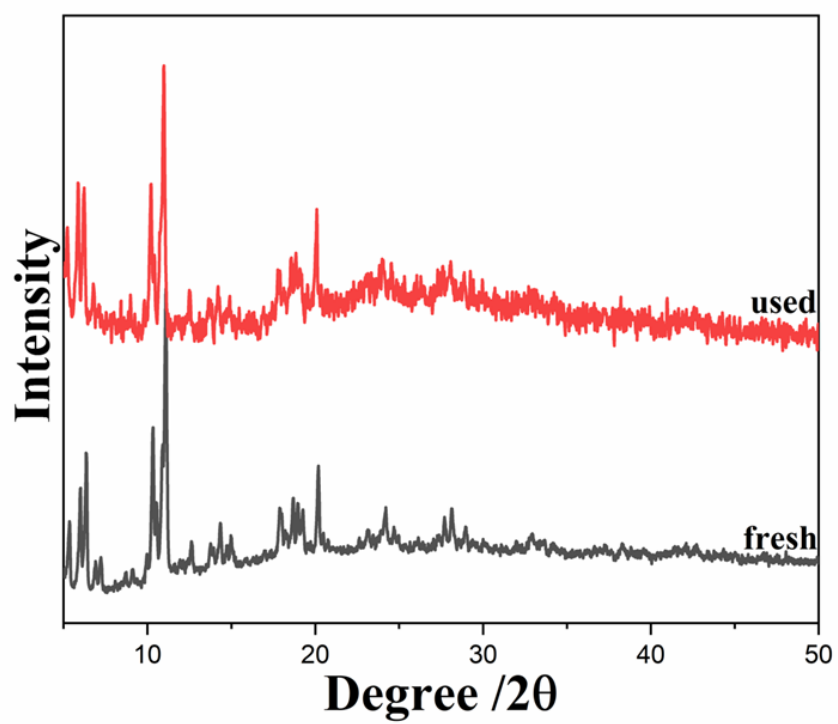


Fig. S21 PXR D patterns of MIL-100(Fe) fresh (black) and after (red) the recycling experiments.

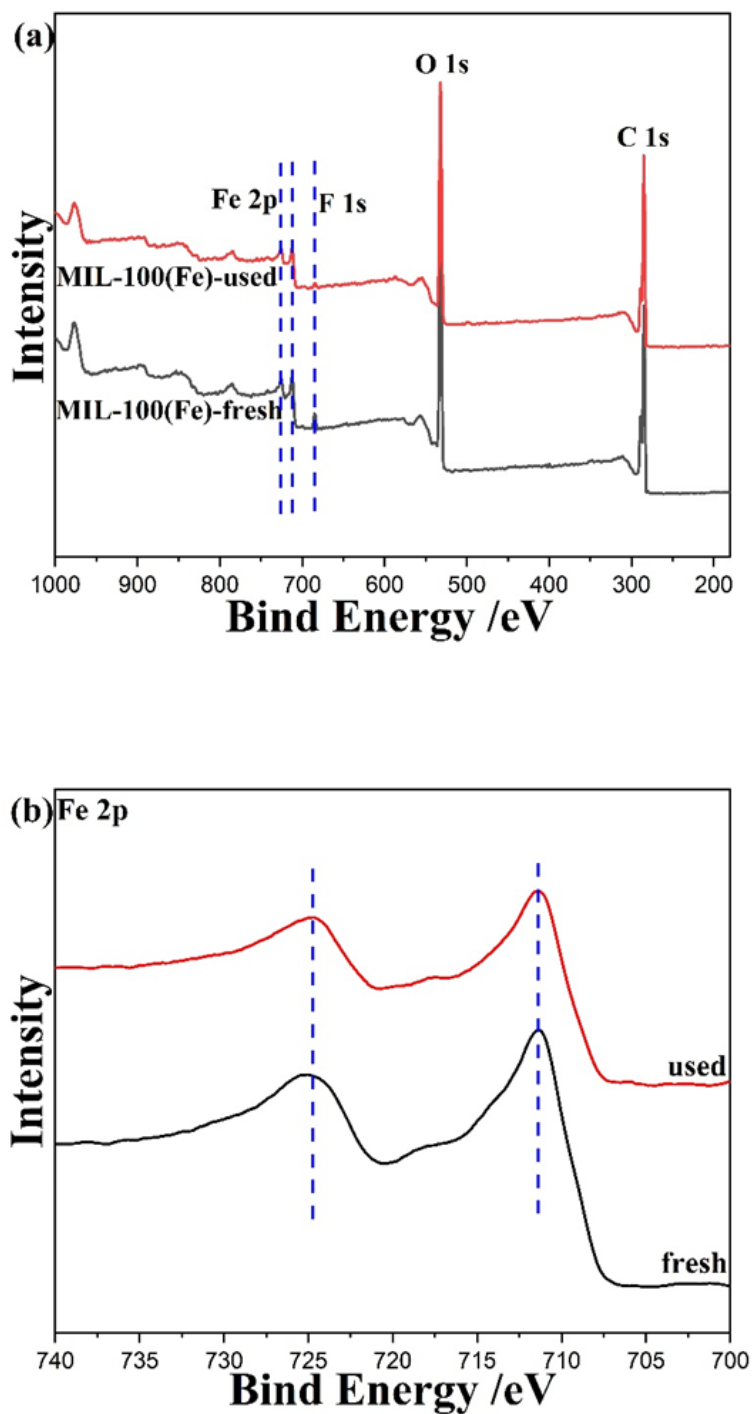


Fig. S22 XPS spectra of MIL-100(Fe) fresh (black) and after (red) after the recycling experiments: (a) survey scan, (b) Fe 2p.

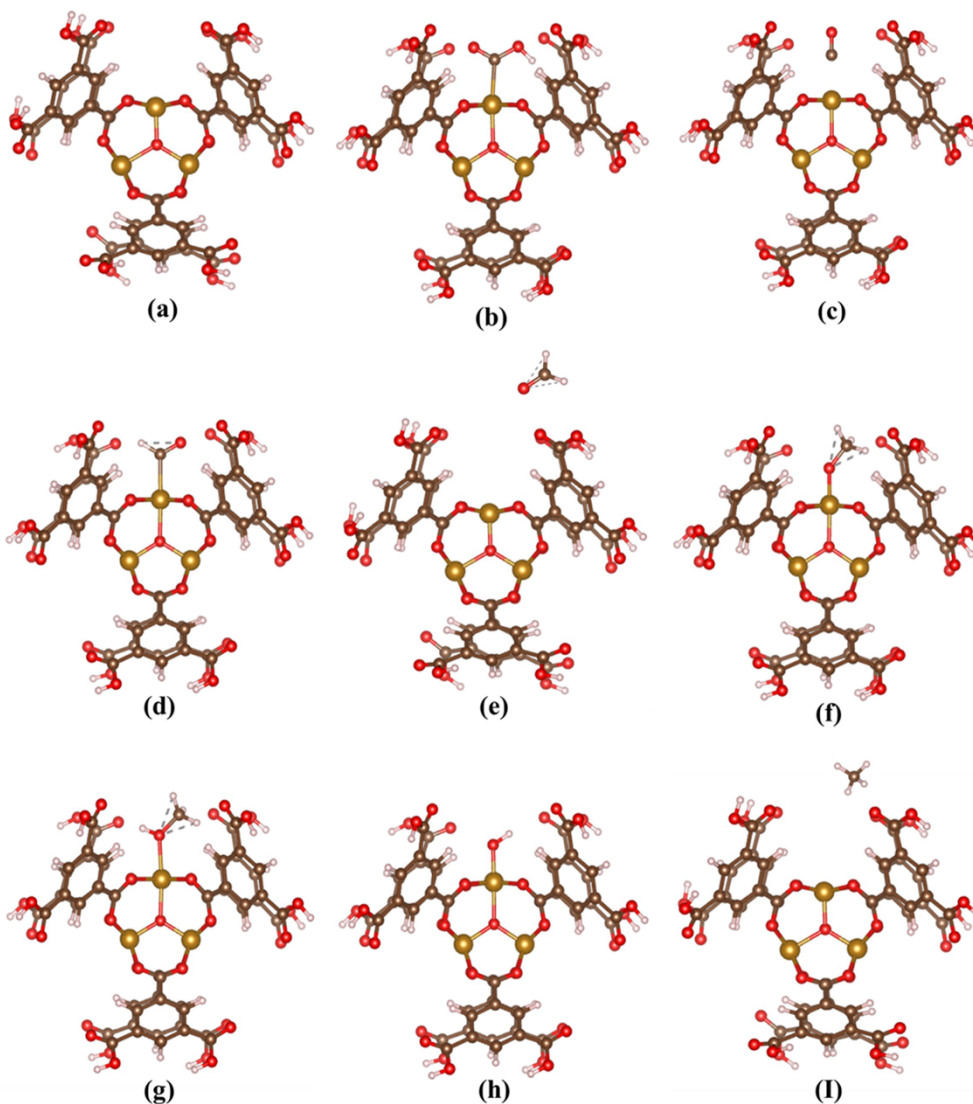


Fig. S23 The optimized geometric structures of intermediates corresponding to the optimal reaction path followed by the CO₂ conversion on MIL-100(Fe): (a) MIL-100(Fe)-CO₂, (b) MIL-100(Fe)-COOH, (c) MIL-100(Fe)-CO, (d) MIL-100(Fe)-CHO, (e) MIL-100(Fe)+CH₂O(g), (f) MIL-100(Fe)-CH₃OH, (g) MIL-100(Fe)-OH, (h) MIL-100(Fe)+CH₄(g).

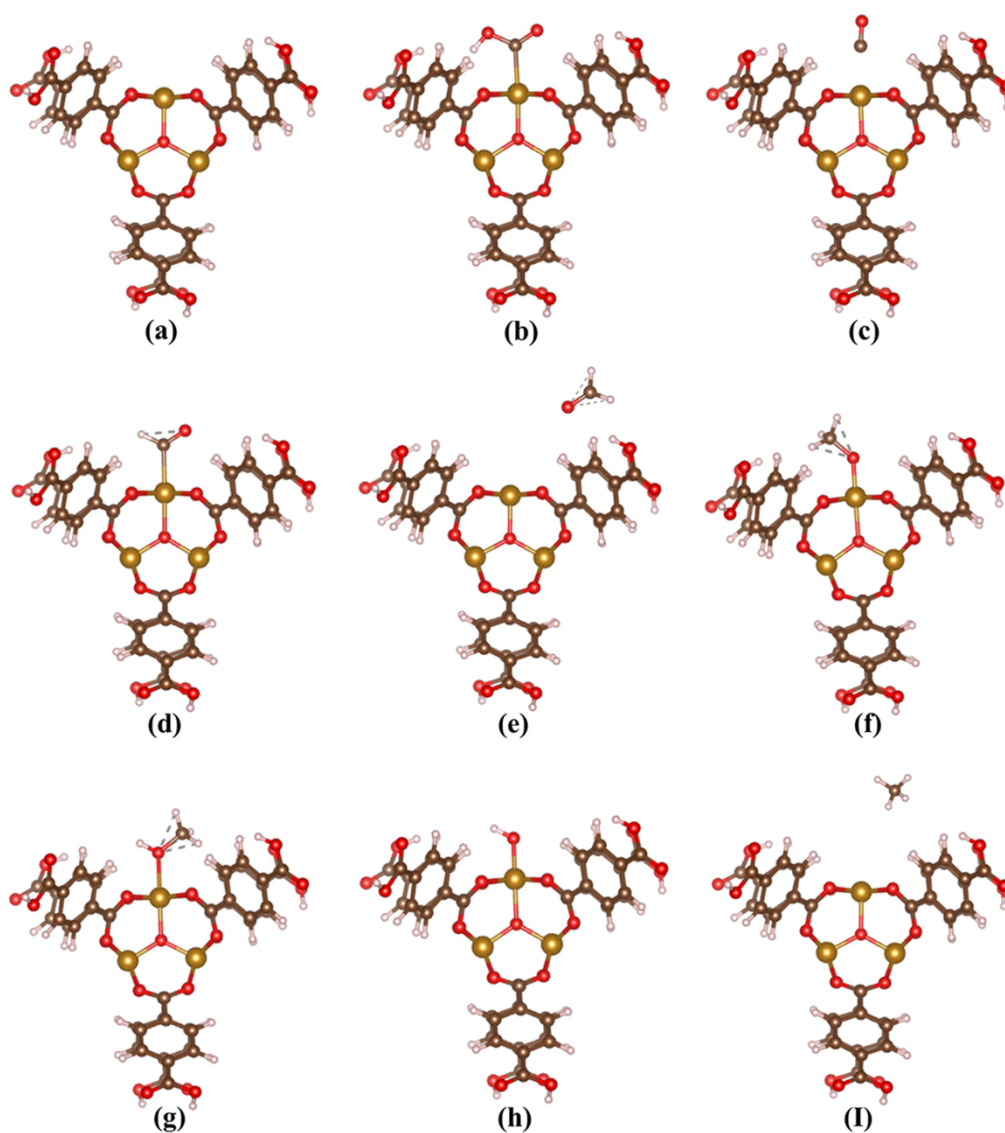


Fig. S24 The optimized geometric structures of intermediates corresponding to the optimal reaction path followed by the CO_2 conversion on MIL-101(Fe): (a) MIL-101(Fe)- CO_2 , (b) MIL-101(Fe)- COOH , (c) MIL-101(Fe)- CO , (d) MIL-101(Fe)- CHO , (e) MIL-101(Fe)+ CH_2O , (f) MIL-101(Fe)- CH_3OH , (g) MIL-101(Fe)- OH , (h) MIL-101(Fe)+ CH_4 .

Table S4. ΔV of the corresponding endothermic process of MIL-100(Fe) and MIL-101(Fe).

	MIL-100(Fe)	MIL-101(Fe)
ΔV_1	1.906 eV	2.005 eV
ΔV_2	1.316 eV	1.463 eV
ΔV_3	0.502 eV	0.541 eV

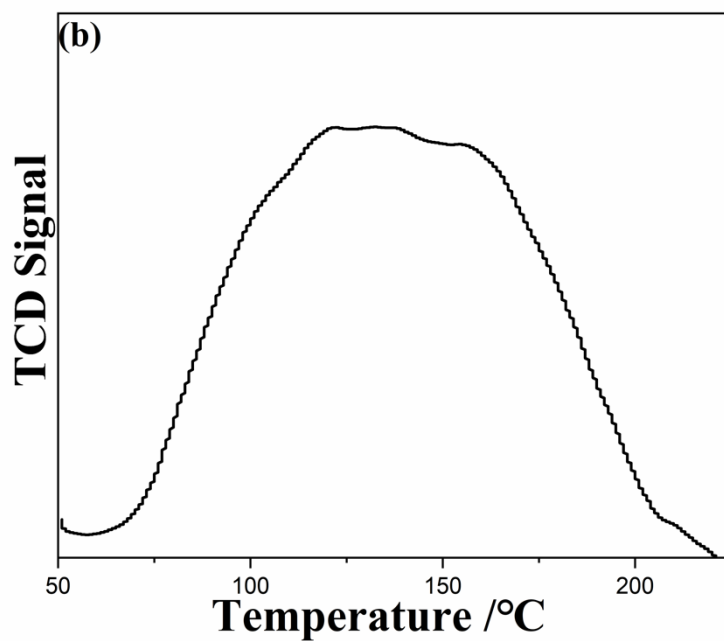
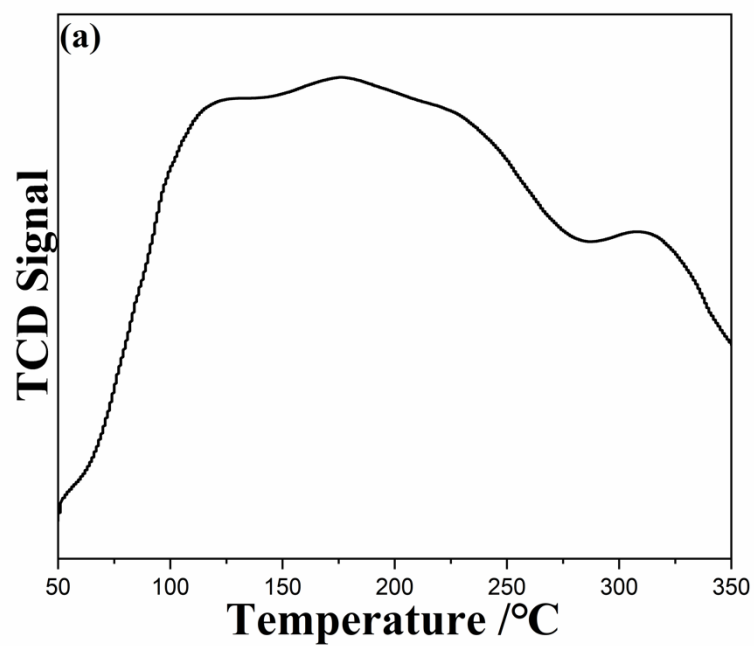


Fig. S25 CO-TPD measurement of MIL-100(Fe) (a) and MIL-101(Fe) (b).

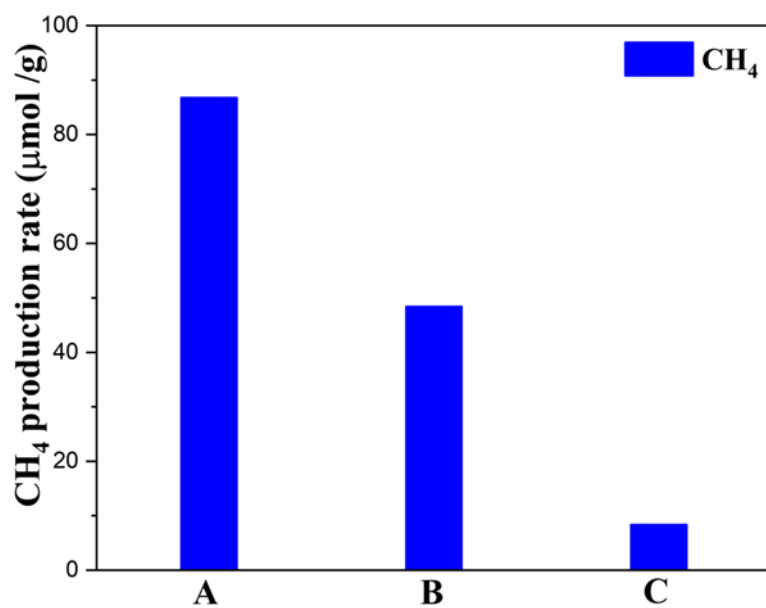


Fig. S26 CO (A), HCHO (B) and CH₃OH (C) were applied separately as feed reactants for CH₄ generation with reaction time 12 h.

References

- 1 P. Horcajada, S. Surble, C. Serre, D. Y. Hong, Y. K. Seo, J. S. Chang, J. M. Greneche, I. Margiolaki, G. Férey, *Chem. Commun.* **2007**, 27, 2822.
- 2 X. Y. Dao, J. H. Guo, Y. P. Wei, F. Guo, Y. Liu, W. Y. Sun, *Inorg. Chem.* **2019**, 58, 8517-8524.
- 3 Y. Mao, H. Qi, G. Ye, L. Han, W. Zhou, W. Xu, Y. Sun, *Microporous Mesoporous Mater.* **2019**, 27, 70-75.
- 4 C. Volkringer, D. Popov, T. Loiseau, G. Férey, M. Burghammer, C. Riekkel, M. Haouas, F. Taulelle, *Chem. Mater.* **2009**, 21, 5695-5697.
- 5 J. A. Mason, K. Sumida, Z. R. Herm, R. Krishna, J. R. Long, *Energy Environ. Sci.* **2011**, 4, 3030-3040.
- 6 X. Li, Y. Sun, J. Xu, Y. Shao, J. Wu, X. Xu, Y. Pan, H. Ju, J. Zhu, Y. Xie, *Nat. Energy* **2019**, 4, 690-699.
- 7 H. Rao, L. C. S. Chmidt, J. Bonin, M. Robert, *Nature* **2017**, 548, 74-77.
- 8 D. Wang, R. Huang, W. Liu, D. Sun, Z. Li, *ACS Catal.* **2014**, 4, 4254.
- 9 Y. Wang, N. Y. Huang, J. Q. Shen, P. Q. Liao, X. M. Chen, J. P. Zhang, *J. Am. Chem. Soc.* **2018**, 140, 38-41.
- 10 Q. Huang, J. Liu, L. Feng, Q. Wang, W. Guan, L. Z. Dong, L. Zhang, L. K. Yan, Y.Q. Lan, H. C. Zhou, *Natl. Sci. Rev.* **2019**, 7, 53.
- 11 T. Nakajima, Y. Tamaki, K. Ueno, E. Kato, T. Nishikawa, K. Ohkubo, Y. Yamazaki, T. Morimoto, O. Ishitani, *J. Am. Chem. Soc.* **2016**, 138, 13818-13821.
- 12 B. Pan, S. Luo, W. Su, X. Wang, *Appl. Catal., B* **2015**, 168, 458-464.